Biosensors and Bioelectronics 50 (2013) 174–179

Contents lists available at SciVerse ScienceDirect

Biosensors and Bioelectronics

journal homepage: www.elsevier.com/locate/bios

Gold microwires based amperometric biosensor exploiting microbial architecture

Shikha Sharma, Sudha Srivastava *

Department of Biotechnology, Jaypee Institute of Information Technology, Noida, UP 201307, India

ARTICLE INFO

Article history:
Received 9 March 2013
Received in revised form
3 June 2013
Accepted 4 June 2013
Available online 1 July 2013

Keywords:
Biosensor
Biocompatible
Microbial architecture
Gold microwires

ABSTRACT

Amalgamation of nanotechnology and biology has opened new horizons for controlled synthesis of nanomaterials of nano and micro-lengthscales for diverse sensing, catalytic and electromechanical applications. Inspired from nature and driven by the need to have nanostructures of desired morphology, microbial architecture has been exploited as a template in the present work. Biocompatible 1-D gold microwires, generated by assembly of amino acid functionalized AuNPs over the proliferating fungal hyphae, served as potential microelectrodes for electron transfer between enzyme and electrode surface. Delocalization of electrons over longer length scales, large surface area provided by assembled AuNPs and high biocompatibility yielded excellent analytical performance characteristics with high sensitivity of 43.2 μA/mM/cm^2 with standard deviation of 0.88% and wide linear range from 5 μM to 20 mM of glucose. The gold microwires thus generated demonstrate appreciable repeatability over 20 cycles in a cyclic voltammogram, and reproducibility with root mean square deviation as low as 1.3%. High stability and biocompatibility attribute these microwires with myriad potential biosensing and catalytic applications in varied domains.

1. Introduction

In recent years, there has been an increased interest in synthesis of one-dimensional (1D) micro/nanostructures of metals and semiconductors (Joshi and Schneider, 2012) due to their unique physical and optical properties with applications in fields like electronics (Du et al., 2012), optics (Cui et al., 2012; Gu et al., 2008), imaging (Cui et al., 2010; Grosges et al., 2008), sensor (Menzel1 et al., 2011; Shen et al., 2012) or biosensor devices (Lu et al., 2012; Huang et al., 2011;Spain et al., 2013). Various synthetic methods have been exploited for synthesis of these 1-D micro-/nanostructures, such as photochemical methods (Lu et al., 2008; Giuffrida et al., 2008; Henglein, 1998), hydrothermal synthesis (Li et al., 2011; Eastman et al., 2011), and hard template (polycarbonate or porous anodic alumina membranes) approach (Yang et al., 2006; Li et al., 2012; Schönenberger et al., 1997). Although the template based synthesis is the most reliable approach among the above mentioned synthesis methods still removal of template in order to obtain pure metallic structures is the major limitation of this approach. Hence it is pertinent to explore eco-friendly route for synthesis of 1D micro/nanostructures. Variety of chemical free reduction methods (using crude extracts of leaf or other natural products), to synthesize gold nanoparticles (AuNPs), has been explored after recognition of amino acids as an independent alternative for reduction of gold ions (Safavi et al., 2012; Wangoo et al., 2008; Toroz and Corni, 2011). Recently, few reports utilizing microorganisms (viruses, bacteria and fungi) as living templates have been proposed for synthesis of different microstructures exploiting unique microbial cell architectures (Rehman et al., 2011; Li et al., 2003; Sugunan et al., 2007). Limited reports available so far, have not been able to understand the mechanism of microwires (MWs) synthesis. Initial studies proposed the probable mechanism of AuNPs assembly on fungal hyphae as solely adsorption driven however later on it was proposed to be nutritional driven. These biological routes of synthesis offer numerous advantages like reduced cost, benign behavior, synthesis of unusual micro or nano-structures, labor-saving approach and are anticipated to overtake the conventional methods.

In the present work, we have exploited the architecture of microorganism for the self-organization of amino acid functionalized AuNPs to synthesize functional microstructures. Driving force being better approachability of nano-/microwires to deeply buried enzyme active centers results in faster electron transfer as demonstrated in our previous work (Sharma et al., 2012). Furthermore, delocalization of electrons over longer length scales in AuMWs, as in case of CNTs and nanowires, is expected to improve the analytical performance of the AuMWs fabricated biosensor. Hence we explored the amino acid functionalized AuMWs for their

* Corresponding author. Tel.: +91 120 2594213; fax: +91 120 2400986.
E-mail address: sudha.srivastava@jiit.ac.in (S. Srivastava).

0956-5663/$ - see front matter © 2013 Elsevier B.V. All rights reserved.
http://dx.doi.org/10.1016/j.bios.2013.06.003

probable biosensing efficiency. Three different fungal species, having different nutritional characteristics, have been used to understand whether MWs synthesis is solely adsorption based or nutritional driven or both. Our work is aimed at understanding the mechanism of synthesis of these functional microstructures of AuNPs and exploring their potential use for efficient biosensor fabrication.

2. Experimental

2.1. Synthesis of AuNPs

Amino functionalized AuNPs were synthesized using two different amino acids (L-Asparagine and L-lysine) as a reducing and capping agent via the chemical reduction method as reported in our previous work (Sharma et al., 2012).

2.2. Fungal inoculation in AuNPs solution

Three different fungal species including *Rhizopus oryzae*, *Penicillium funiculosum*, and *Aspergillus parasiticus*, were inoculated in three different flasks containing liquid media with KH_2PO_4 (7.0 g/l), K_2HPO_4 (2.0 g/l), $MgSO_4.7H_2O$ (0.1 g/l), $(NH_4)_2SO_4$ (1.0 g/l), yeast extract (1.0 g/l), and glucose (1.0 g/l) so as to promote the spore formation. The flask was incubated at 30 °C for 4 days in a rotary orbital shaker. The spores were harvested and washed with distilled water to remove any medium component. Number of spores were calculated with haemocytometer to ensure equal inoculum in all the tubes. Finally, 5×10^6 spores/ml of *R. oryzae*, *P. funiculosum*, and *A. parasiticus*, were mixed in 10 ml of aqueous solution of AuNPs in three different tubes—1, 2 and 3, respectively maintained at 30 °C. The spores started germinating after about 24 h, and the red growing fungal biomass was clearly visible within 48–72 h. After 1 week fungal biomass was harvested and washed thrice with distilled water, followed by sonication in ultrasonic bath for 15 min to remove any unbound AuNPs. Fungus was heat killed at 90 °C for 15 min and dry cell weight calculated as 10 mg (*R. oryzae*), 9.2 mg (*P. funiculosum*) and 6 mg (*A. parasiticus*). All the experiments were conducted in triplicates and results reported as average of triplicates.

2.3. Fabrication of AuMWs functionalized electrode

Fig. 1 shows schematic representation of AuMWs based biosensor fabrication. The working electrode was modified by addition of 10 μl of 3-APT (2.5 mM) solution and was air dried. The thiol group of 3-APT binds to the Au surface, while the amino group remains free for attachment to other groups. Functionalized electrode was rinsed thoroughly with distilled water to remove physically adsorbed 3-APT. This was followed by addition of 10 μl of glutaraldehyde (2.5%) was dropped onto the 3-APT modified electrode and kept for 4 h to ensure the interaction of free NH_2 of 3-APT and CHO of glutaraldehyde. These AuMWs were covalently immobilized onto activated gold surface through interaction NH_2 of AuMWs and CHO terminated gold surface. This was followed by immobilization of 20 units of glucose oxidase enzyme (GOx) onto the AuMWs modified electrode surface.

3. Results and discussion

AuNPs functionalized with amino acids (L-Lysine) were prepared via eco-friendly route, in order to reduce the complexity of current methodologies and to avoid the usage of toxic materials as reducing and capping agent. The amino acid and high temperature are the key factors that facilitate the formation of nuclei and control the growth of nanoparticles. Amino acid induced reduction of yellow colored $HAuCl_4$ solution led to formation of ruby red solution of AuNPs. This was further confirmed by UV–vis spectrophotometric analysis as indicated by the presence of fairly narrow characteristic plasmon absorption band of AuNPs at 523 nm while the remainder unreacted $HAuCl_4$ precursor in solution is identified by absorption peak at 300–310 nm (see Fig. S1(A) in Supplementary materials). Transmission electron microscopic examination of these particles showed fairly uniform shape and a narrow size distribution of 10–20 nm (see Fig. S1(B) in Supplementary materials). The synthesized AuNPs solution was divided equally into three tubes—1, 2 and 3, ensuring same concentration of AuNPs

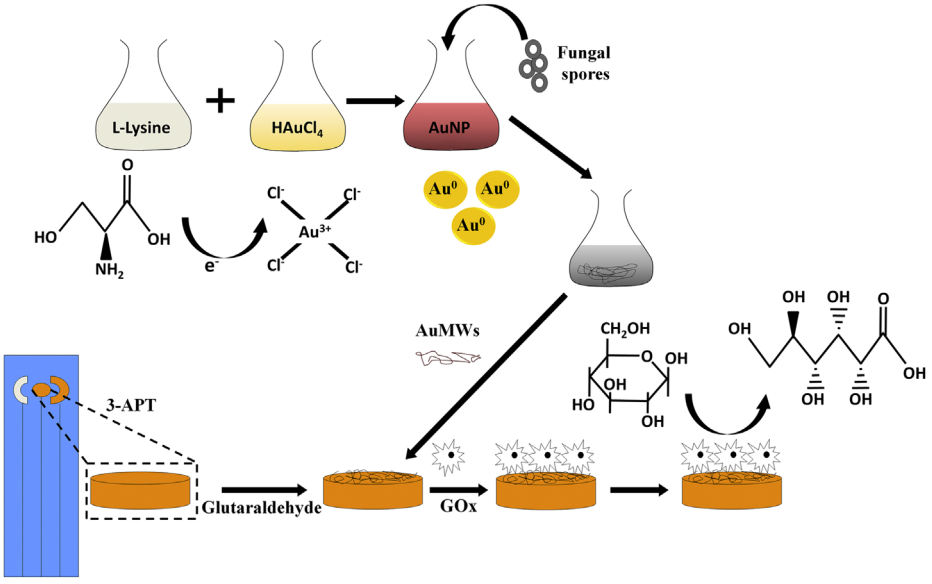

Fig. 1. Schematic representation of AuMWs based biosensor fabrication.

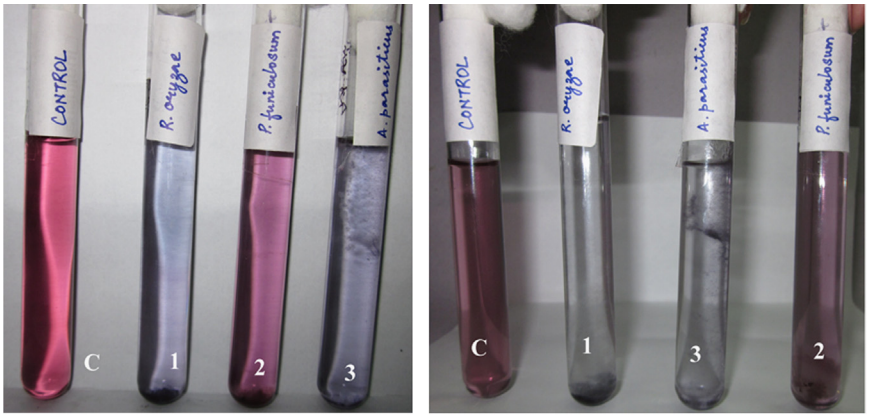

Fig. 2. Depletion of AuNPs from the colloidal solution after 72 h and 1 week of inoculation of fungal spores of *R. oryzae* (tube 1), *P. funiculosum* (tube 2) and *A. parasiticus* (tube 3). Tube C is negative control with AuNPs solution only.

solution. The fungal spores (5×10^6 spores/ml) of *R. oryzae*, *P. funiculosum*, and *A. parasiticus* were inoculated in the aqueous solution of AuNPs at 30 °C under aseptic conditions without addition of any additional nutrients. The negative control was taken as AuNPs solution only i.e., no fungal spores (tube C) as shown in Fig. 2. After 2 days fungal biomass started appearing in all the tubes which gradually increased with time over a period of one week. The *Rhizopus* and *Aspergillus* fungus in both tubes 1 and 3 showed a reddish purple mass, accompanied by a significant decrease in red color of the colloidal solution with increasing time. Variation in color of colloidal solution after 72 h of inoculation of fungal spores and later after 1 week is shown in Fig. 2.

3.1. Absorption spectroscopic studies

The time dependent analysis of growing fungal hyphae in AuNPs colloidal solution was studied using absorption spectroscopy. As seen in Fig. 3(a) and Fig. S2 in Supplementary materials, the characteristic plasmon band of AuNPs shows a gradual decrease with time which finally disappears after 1 week. Fig. 3(b) showed only slight variation in peak position with time up to 72 h followed by no further change in peak intensity. The variation in color of the colloidal solution is a direct outcome of depletion of freely suspended AuNPs in the solution, thus indicating drifting out of AuNPs from the solution and their assembly onto the growing fungal hyphae. This is marked by appearance of reddish purple biomass at the bottom of the tubes (tubes 1 and 3). Whereas, the slight red shift in plasmon in solution from tube 2 containing growing *P. funiculosum* is simply due to initial agglomeration of NPs as a result of destabilization of amino acid coated NPs. While negative control tube C showed almost no change in absorption peak initially, though towards the end of week there was slight broadening of the peak due to settling down and agglomeration over a prolonged period. The change in peak intensity was marginal.

3.2. Optical and electron microscopic characterization of AuMWs

The fungal mycelium was harvested from all three test tubes 1, 2 and 3 and was observed under an optical microscope. Fig. S3(A–C) in Supplementary materials shows optical images of *A. parasiticus*, *P. funiculosum* and *R. oryzae* respectively and inset shows enlarged image of selected region. Optical images of *A. parasiticus* and *R. oryzae* show 80–90% fungal hyphae dark in color showing the probable attachment of AuNPs while ~10–20% were partially hollow tubular hyphae as evident from transparent or light colored hyphae.

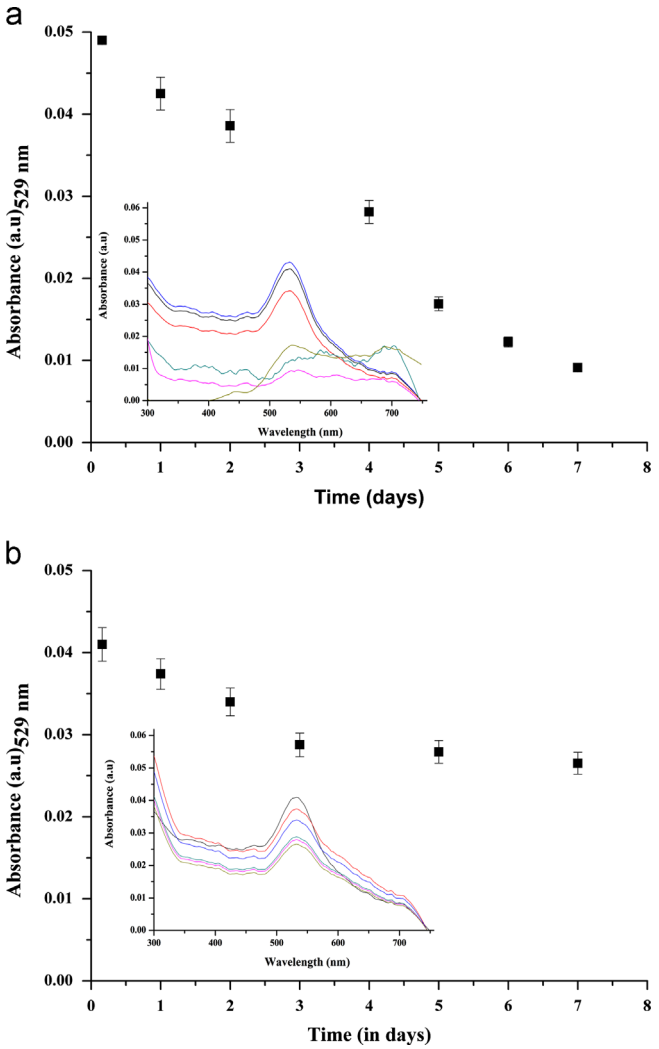

Fig. 3. Variation in absorbance maxima of AuNPs with time during growth of the mycelium (A) *A parasiticus* and (B) *P. funiculosum*, in AuNPs solution. Inset shows corresponding UV–vis absorption spectra. Results are average of experiments performed in triplicates with RSD of 1.86% for *A parasiticus* and 2.1% for *P. funiculosum*.

These results were further corroborated with scanning electron microscopy equipped with an energy dispersive X-ray (EDX) detectors and TEM mapping confirming the nanoparticle/fungal hyphae

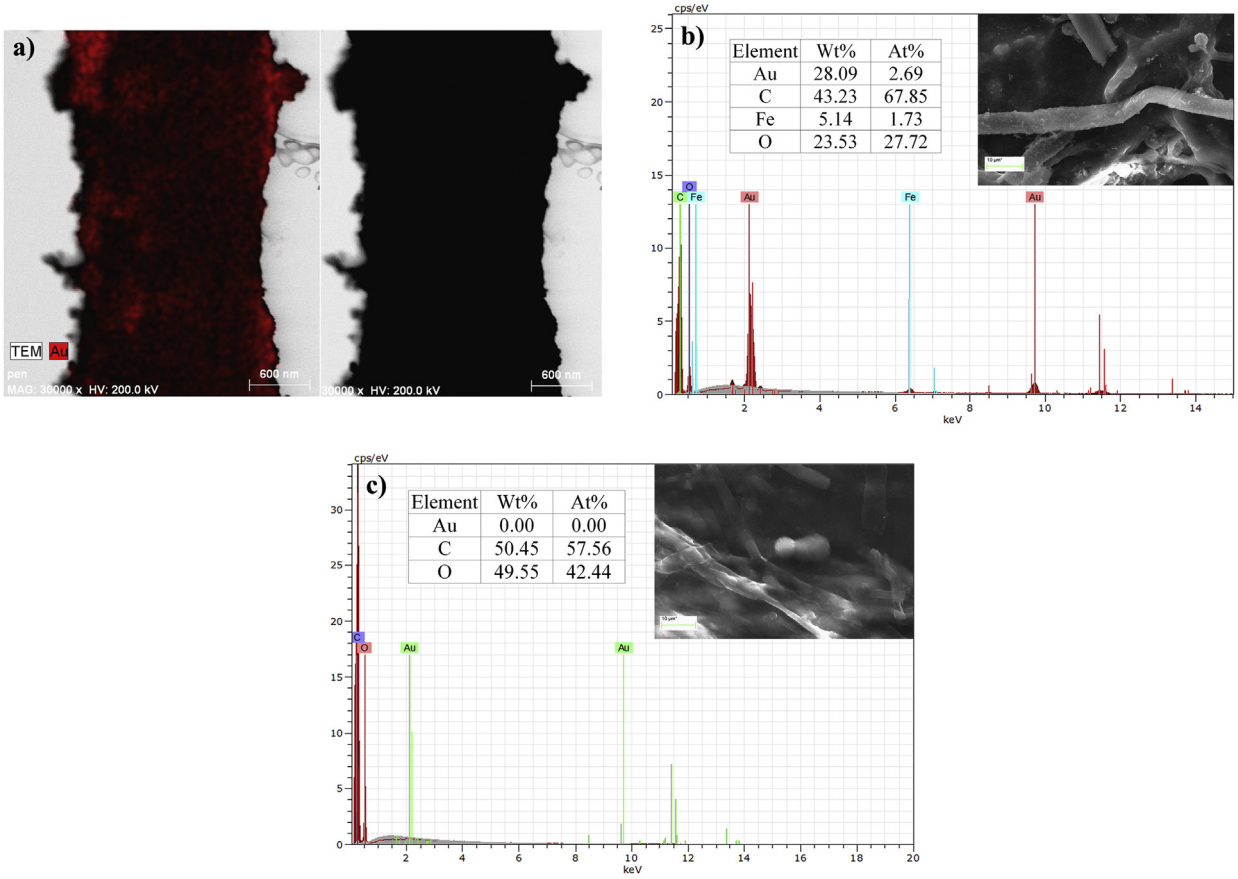

Fig. 4. (A) TEM mapping showing AuNPs (red colored dots) covered surface of *R. oryzae* while EDX spectra of mycelia showing elemental analysis of (B) *A. parasiticus, and* (C) *P. funiculosum,* after 1 week of growth in AuNPs solution. Inset shows corresponding SEM micrographs and percentage of each of the atoms. (For interpretation of the references to color in this figure legend, the reader is referred to the web version of this article.)

structure. Fig. 4a shows TEM mapping showing red AuNPs (red colored dots) covered *R. oryzae* fungal hyphae.

Elemental analysis using energy dispersive X-ray spectroscopy (EDX) of fungal hyphae decorated with gold nanoparticles confirmed 28% of gold on the hyphae surface in case of *A. parasiticus* (Fig. 4b) and 24% of gold for *R. oryzae* (Fig. S4 in Supplementary materials), whereas no gold nanoparticles were observed (0% Au) on the hyphae surface of *P. funiculosum* (Fig. 4c). Inset shows the corresponding SEM micrographs without coating the fungus with any conductive material. SEM image of *P. funiculosum* in comparison to the other two fungus lacked the clarity and sharpness probably because of the absence of gold nanoparticles. The EDX results are in agreement with utilization rate or rate of depletion of AuNPs from solution of different species of fungi shown in Fig. 3(a–c).

3.3. Proposed mechanism

As discussed earlier, limited number of reports are available on MWs synthesis using bio-templates. Moreover, no clear mechanism of such an assembly of AuNPs has been proposed so far. In order to understand the interaction between the fungal biomass and AuNPs attached onto its surface, the harvested mass from all the test tubes was washed 3–4 times with distilled water and further sonicated in order to remove all unbound nanoparticles. Most microorganisms possess net negative charge at physiological pH as the number of carboxylic and phosphate groups dominate their surface as compared to amino groups. The fungus initially grows on the unutilized free amino acids present in the AuNPs solution, since no additional nutrients were available. Once the free amino acids are depleted from the solution, fungal biomass starts attracting amino acid coated AuNPs for their further growth. Interaction of microorganism with the amino groups of AuNPs leads to formation of peptide bond with carboxylic group present on the fungi surface. This theory of initial utilization of free amino acids and later on the amino acid coated AuNPs is also supported by the fact that during initial growth a white cottony fungal mass was observed even in tubes 1, 2 and 3. As the time progressed, the color of the fungal mass changed to red that eventually became purple in color. Moreover, partially covered and partially hollow hyphal structures as observed in optical images could be ascribed to the growing fungal species. As the fungus grows it picks up the amino coated AuNPs for its further growth as it utilizes amino acids as nitrogen source for growth, in this process the AuNPs form the peptide bond with the functional groups present on hyphae surface. The above studies demonstrate the formation of these gold microstructures to be nutritional driven process and further peptide bond ensures the stability of the structure. However, the studies with *P. funiculosum* again demands further confirmation for nutritional driven synthesis of these microstructures. The fact that *P. funiculosum* utilizes asparagine as nitrogen source was exploited to synthesize L-Asparagine functionalized AuNPs for further studies. Utilization of L-Asparagine functionalized AuNPs by *P. funiculosum* confirmed the nutritional driven hypothesis.

3.4. Biosensing performance analysis

3.4.1. Electrochemical impedance spectroscopic studies

The alteration in electron-transfer resistance of the conductive electrode due to immobilization of AuMWs and GOx was studied

using EIS. Fig. S5 in Supplementary materials, shows the impedance spectra of bare gold electrode (curve a), AuMWs modified electrode (curve b), and after immobilization of glucose oxidase on AuMWs modified electrode (curve c), respectively and the equivalent circuit is shown in inset. The bare gold electrode shows an electron transfer resistance (R_{ct}) value of 140 Ω. R_{ct} changed to 136 Ω with modification of bare electrode with AuMWs, indicating the decreased resistance to the flow of electrons at the electrode surface interface. The increased R_{ct} value of 256 Ω after immobilization of glucose oxidase could be attributed to the hydrophobic layer of the protein which acted as an insulator on the surface of conductive electrode surface.

3.4.2. Electroactive surface area of the electrode

Relative change in electroactive surface area of bare Pt electrode and AuMWs/Pt electrode was estimated from the Randles–Sevcik equation for peak current at room temperature

$$I_p = (2.65 \times 10^5) n^{3/2} A C D^{1/2} \upsilon^{1/2}$$

where, I_p is peak current (A), n is number of electron transfer in redox reaction, A is electrode surface area (cm^2), D is diffusion coefficient (cm^2/s), C is concentration of diffusing species (mol/cm^3) and ν is scan rate (V/s). The geometrical surface area of the electrode is 0.14 cm^2. The effect of AuMWs modification on electrode surface area was evaluated from the ratio of peak current of bare Pt electrode (12.5 μA) and AuMWs/Pt electrode (23 μA) (as shown in Fig. S6 in Supplementary materials)

$$I_p(\text{AuNP/Pt electrode})/I_p(\text{bare Pt electrode}) = A'/A$$

as 1.8. This increased electroactive surface area as a result of AuMWs modification of Pt electrode ensures increased enzyme loading capacity and hence holds promise of increased sensitivity and lower detection limits of the fabricated biosensor.

3.4.3. Cyclic voltammetric measurements

Fig. 5 shows the CV studies of GOx/AuMWs modified Pt electrode as a function of scan rate varying from 10 to 100 mV s^{-1}. The variation of the redox peak height with sweep rate is shown in inset. The linear variation of I_p vs $\upsilon^{1/2}$ is indicative of the direct electron transfer process between the enzyme and the electrode surface. In other words, AuMWs served as a good candidate for modification of electrode assisting the easy shuttling of electrons between the enzyme and the electrode representing the phenomenon equivalent to direct electron transfer. The electron transfer rate constant (k_s) and cathodic transfer coefficient (α) was calculated using Laviron's equation from the slope of the curve for E_P vs ln(υ). The electron transfer rate was found to be 2.8 s^{-1}

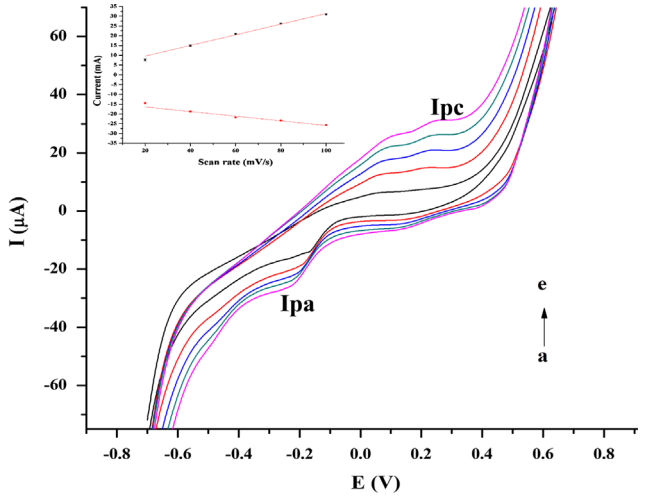

Fig. 5. Cyclic voltammogram of GOx–AuMWs modified electrode for scan rate varying from 10 to 100 mV s^{-1} in 0.1 M phosphate buffer pH 7.4; inset shows linear variation of anodic and cathodic peak current with an RSD value of 1.32%.

3.4.4. Amperometric measurements

The amperometric responses of the GOx/AuMWs modified gold electrode for different glucose concentrations at 0.15 V, presented in Fig. S7(A–B) in Supplementary materials shows the linear variation of the same over the concentration range from 5 μM to 20 mM. The response current follows Michaelis–Menten behavior with increasing glucose concentration. The apparent Michaelis–Menten constant $K_{m,app}$ was calculated from the slope of this straight line using the Lineweaver–Burk plot of I^{-1} vs $[\text{glucose}]^{-1}$. Thus, a smaller $K_{m,app}$ value of 3.6 mM suggests high affinity of the enzyme for the substrate. The amperometric sensitivity of the GOx/AuMWs gold electrode was 43.2 μA/mM/cm^2 with a linear range from 5 μM to 20 mM glucose. The detection limit of the AuMWs modified gold electrode was found to be 5 μM and a steady-state response current was generated within 6 s.

3.4.5. Precision

Precision of the fabricated biosensor was evaluated in terms of reproducibility and repeatability. The reproducibility of the amperometric signal was checked using three sets of identical biosensors and calculating the slope of the calibration curve for each. The RSD values obtained were 1.3%. The obtained results ensure good reproducibility of the GOx/AuMWs modified electrode. The repeatability of the biosensor was evaluated by repeating the CV over the studied potential range for twenty cycles. Repeatability was also evaluated by performing five consecutive measurements on each of the biosensors at 0.15 V for 10 mM glucose in phosphate buffer pH 7.4. RSD and was found to be 1.8%.

3.4.6. Storage stability

Storage stability of a biosensor is one of the critical parameter for transferring a biosensor from lab to market. Therefore, in the present study the fabricated biosensor was stored at 4 °C in order to avoid deactivation of the immobilized enzyme. The response current was measured from time to time for 90 days. The biosensor response current is plotted as a function of time in Fig. S8 in Supplementary materials. As observed from figure, the biosensor remained stable for 90 days retaining approximately 60% of its initial response current. The good stability of the biosensor could be attributed to the strong interaction between GOx and AuMWs.

4. Conclusions

Here, we have demonstrated the synthesis of AuMWs of micrometer length scales using microorganism (fungal hyphae) as template. This approach allows the synthesis of nano-/micro-structures of desired morphology by appropriate choice of microorganism and allowing them to grow in amino acid functionalized NPs solution. These biocompatible nano-/micro-structures showed good reproducibility and repeatability promising potential for myriad applications. In the present work we have developed a glucose biosensor that shows a wide linear range from 5 μM to 20 mM and sensitivity of 43.2 μA mM^{-1} cm^{-2}. Biosensor retained 75% of its activity up to 60 days with K_m as 3.6 mM and the electron transfer rate was 2.8 s^{-1}. The reduced working potential (0.15 V) required for AuMWs based glucose biosensor ensures no interference from other electroactive species. We expect that the stability and sensitivity can be further improved by ensuring vertically aligned AuMWs rather than random orientation as was the case in present study.

Acknowledgments

This project was funded by All India Council for Technical Education (AICTE) (File no. 8023/BOR/RID/RPS-68/2008-09). We are thankful to the Biosensors Laboratory, Institute of Microbial Technology (IMTECH), Chandigarh for allowing us to use the cyclic voltammetry facility. Advanced Instrumentation Research Facility (AIRF), Jawaharlal Nehru University, New Delhi is gratefully acknowledged for providing access to TEM and SEM facility. Shikha Sharma is thankful to JIIT University for providing research fellowship.

Appendix A. Supporting information

Supplementary data associated with this article can be found in the online version at http://dx.doi.org/10.1016/j.bios.2013.06.003.

References

Joshi, R.K., Schneider, J.J., 2012. Chemical Society Reviews 41, 5285–5312.
Du, N., Zhang, H., Yang, D., 2012. Nanoscale 4, 5517–5526.
Cui, Q.H., Zhao, Y.S., Yao, J., 2012. Journal of Material Chemistry 22, 4136–4140.
Gu, F., Zhang, L., Yin, X., Tong, L., 2008. Nano Letters 8, 2757–2761.
Cui, X., Tawa1, K., Kintaka, K., Nishii, J., 2010. Advanced Functional Materials 20, 945–950.
Grosges, T., Barchiesi, D., Toury, T., Gréhan, G., 2008. Optics Letters 33, 2812–2814.
Menzel1, A., Subannajui, K., Güder, F., Moser, D., Paul, O., Zacharias, M., 2011. Advanced Functional Materials 21, 4342–4348.
Shen, F., Wang, J., Xu, Z., Wu, T., Chen, Q., Li, X., Jie, X., Li, L., Yao, M., Guo, X., Zhu, T., 2012. Nano Letters 12, 3722–3730.
Lu, X., Dong, X., Zhang, K., Han, X., Fang, X., Zhang, Y., 2012. Analyst 138, 642–650.
Huang, H., Liu, X., Liao, B., Chu, P.K., 2011. Plasmonics 6, 1–9.
Spain, E., Keyes, T.E., Forster, R.J., 2013. Biosensors and Bioelectronics 41, 65–70.
Lu, W., Jin, Y., Wang, G., Chen, D., Li, J., 2008. Biosensors and Bioelectronics 23, 1534–1539.
Giuffrida, S., Costanzo, L.L., Ventimiglia, G., Bongiorno, C., 2008. Journal of Nanoparticle Research 10, 1183–1192.
Henglein, A., 1998. Chemistry of Materials 10, 444–450.
Li, J., Wan, W., Zhou, H., Li, J., Xu, D., 2011. Chemical Communications 47, 3439–3441.
Eastman, M., Besser, A., Chen, Y., Jiao, J., 2011. Journal of Physical Chemistry C 115, 10979–10984.
Yang, Z., Huang, Y., Dong, B., Li, H.L., Shi, S.Q., 2006. Applied Physics A 84, 117–122.
Li, X., Wang, Y., Lei, Y., Gu, Z., 2012. RSC Advances 2, 2302–2307.
Schönenberger, C., Zande, B.M.I., Fokkink, L.G.J., Henny, M., Schmid, C., Krüger, M., Bachtold, A., Huber, R., Birk, H., Staufer, U., 1997. Journal of Physical Chemistry B 101, 5497–5505.
Safavi, A., Zeinali, S., Yazdani, M., 2012. Amino Acids 43, 1323–1330.
Wangoo, N., Bhasin, K.K., Mehta, S.K., Suri, C.R., 2008. Journal of Colloid and Interface Science 323, 247–254.
Toroz, D., Corni, S., 2011. Nano Lett. 11, 1313–1318.
Rehman, A., Majeed, M.I., Ihsan, A., Hussain, S.F., Rehman, S.U., Ghauri, M.A., Khalid, Z.M., Hussain, I., 2011. Journal of Nanoparticle Research 13, 6747–6754.
Li, Z., Chung, S.W., Nam, J.M., Ginger, D.S., Mirkin, C.A., 2003. Angewandte Chemie International Edition 42, 2306–2309.
Sugunan, A., Melin, P., Schnürer, J., Hilborn, J.G., Dutta, J., 2007. Advanced Materials 19, 77–81.
Sharma, S., Gupta, N., Srivastava, S., 2012. Biosensors and Bioelectronics 37, 30–37.